POLITECNICO DI TORINO
Repository ISTITUZIONALE

Electrospun rubber nanofibrous membranes with thiol functionalization for heavy metal removal and detection

Original
Electrospun rubber nanofibrous membranes with thiol functionalization for heavy metal removal and detection / Vu, T.N., Quaglio, M., Bongiovanni, R., Vitale, A.. - In: CHEMICAL ENGINEERING JOURNAL ADVANCES. - ISSN 2666-8211. - ELETTRONICO. - 27:(2026), pp. 1-11. [10.1016/j.ceja.2026.101383]

Availability:
This version is available at: 11583/3016191 since: 2026-10-01T08:50:55Z

Publisher:
Elsevier

Published
DOI:10.1016/j.ceja.2026.101383

Terms of use:

This article is made available under terms and conditions as specified in the corresponding bibliographic description in the repository

Publisher copyright

(Article begins on next page)

18 November 2026

Chemical Engineering Journal Advances 27 (2026) 101383

Contents lists available at ScienceDirect

Chemical Engineering Journal Advances

journal homepage: www.sciencedirect.com/journal/chemical-engineering-journal-advances

Electrospun rubber nanofibrous membranes with thiol functionalization for heavy metal removal and detection

Thi Nhung Vu *, Marzia Quaglio, Roberta Bongiovanni, Alessandra Vitale *

Department of Applied Science and Technology, Politecnico di Torino, 10129, Torino, Italy

ARTICLE INFO

Keywords:
Functionalized membranes
Suspension electrospinning
Thiol-ene click chemistry
Photo-induced surface functionalization
Heavy metal adsorption
Water treatment

ABSTRACT

This work presents a sustainable strategy for fabricating thiol-functionalized electrospun nanofibrous membranes (ENMs) for heavy metal removal and detection in water. The membranes are produced via green electrospinning of an aqueous styrene–butadiene rubber (SBR)/poly(ethylene oxide) (PEO) dispersion, followed by UV irradiation that simultaneously induces thiol-ene crosslinking and surface functionalization. This process stabilizes the nanofibrous structure while enabling precise control of the surface density of accessible thiol (-SH) groups through stoichiometric tuning, reaching values of approximately 180 μmol/g. The resulting ENMs exhibit effective interaction with multiple heavy metal ions (i.e., Cu(II), Pb(II), Hg(II), and Ag(I)), combining adsorption capability with colorimetric detection in aqueous media. A distinct response toward Cu(II) allows detection down to 3 mg/L. The nanofibrous architecture enhances functional group accessibility compared to dense materials, while maintaining mechanical robustness and favorable wettability for operation in aqueous environments. This solvent-free, low-energy approach provides a scalable and environmentally benign route to multifunctional nanofibrous membranes with tunable surface chemistry and dual detection–removal functionality, highlighting their potential for advanced water treatment and monitoring applications.

1. Introduction

Electrospun nanofibrous membranes (ENMs) represent a significant advancement in membrane technology due to their high specific surface area, interconnected porous structure, and tunable surface chemistry [1]. These features enable enhanced mass transport, high permeability, and efficient interfacial interactions, which are critical for separation and adsorption-based processes. Electrospinning is a versatile and well-established technique for producing continuous nanofibers with diameters down to the nanoscale by applying a high electric field to a viscoelastic fluid jet [2]. This process allows the formation of nonwoven fibrous membranes with controllable thickness, porosity, and fiber alignment. A key advantage of electrospinning is its exceptional material versatility, enabling the fabrication of nanofibers from a wide range of feedstocks, including biobased and synthetic polymers as well as organic and inorganic systems [3,4]. Furthermore, the electrospinning process allows precise control of fiber morphology and membrane architecture by carefully adjusting solution properties, processing parameters, and fabrication conditions [5,6]. As a result, ENMs find applications in diverse fields, such as energy storage, biomedical devices, textiles, and, notably, water treatment technologies [7–10]. In the context of water purification, their high surface-area-to-volume ratio, interconnected pore network, and ease of surface functionalization make ENMs particularly attractive for the removal and detection of dissolved contaminants, including heavy metal ions [11].

Among the various electrospinning approaches, suspension electrospinning has emerged as a particularly green and versatile technique [12], as it employs aqueous colloidal suspensions or dispersions rather than polymer solutions that often require organic solvents or melt processing at elevated temperatures. This water-based methodology significantly reduces environmental impact while expanding the range of processable materials, including latex systems and particle-based formulations. In addition, crosslinking strategies can be integrated with electrospinning, either during or after fiber formation, to enhance mechanical integrity and introduce targeted surface functionality [13,14]. Our previous work has demonstrated that suspension electrospinning combined with photo-induced crosslinking enables the fabrication of rubber-based nanofibrous membranes with unique morphologies, improved structural stability, and tunable physicochemical properties, while maintaining a fully water-based and sustainable

* Corresponding authors.
E-mail addresses: thi.vu@polito.it (T.N. Vu), alessandra.vitale@polito.it (A. Vitale).

https://doi.org/10.1016/j.ceja.2026.101383

Available online 16 July 2026
2666-8211/© 2026 The Authors. Published by Elsevier B.V. This is an open access article under the CC BY license (http://creativecommons.org/licenses/by/4.0/).

processing route [15].

Building on this strategy, the present study describes a sustainable and efficient approach for fabricating functionalized ENMs based on styrene-butadiene rubber (SBR) latex. Poly(ethylene oxide) (PEO) is employed as a sacrificial template to facilitate fiber formation, while a multifunctional thiol acts as both a crosslinker and a surface functionalization agent. Upon UV irradiation, a "click" thiol-ene hydrothiolation reaction occurs between the thiol groups of the crosslinker and the C=C double bonds of the SBR backbone [16–19], generating a stable three-dimensional fibrous network. This photo-induced crosslinking effectively suppresses cold flow and enhances the morphological stability, mechanical integrity, and chemical resistance of the membranes, while allowing removal of the PEO template without loss of the nanofibrous structure [20].

Most importantly, control over the thiol-ene stoichiometry enables the introduction of free thiol (–SH) functional groups on the fiber surface. Among commonly used functional groups for water treatment applications, such as -NH_2, -COOH, and -SO_3H, thiol groups are particularly attractive due to their strong affinity and selective binding toward heavy metal ions, forming stable metal-sulfur complexes [21]. As soft Lewis bases, thiol groups preferentially interact with soft Lewis acid metal ions through coordinate covalent bonding [22–24]. This interaction is especially relevant for toxic, non-biodegradable heavy metals such as mercury (Hg) and lead (Pb), which are widely recognized as priority pollutants [3,5]. These metals can enter the human body through contaminated drinking water and the food chain and may cause severe health effects, including metabolic dysfunction, organ toxicity, and chronic diseases, due to their strong interactions with biological molecules [1,5,25,26]. To address the issue of contaminated water threatening human health, ecosystems, and environmental integrity, several water purification technologies are currently employed, including chemical precipitation and ion exchange [27,28]. However, these methods often suffer from limitations such as low efficiency, high reagent consumption, and the generation of secondary toxic wastes [29, 30]. Filtration and adsorption-based approaches offer distinct advantages [31], particularly when the filtering materials combine efficient mass transport with strong, selective binding sites. In this context, functionalized ENMs are particularly promising, as their porous fibrous architecture enables physical sieving of particulate contaminants, while tailored surface chemistry allows selective binding of metal ions, even at very low concentrations [32–34]. Moreover, ENMs can offer high removal efficiency, low operating pressure, high permeation flux, and potential for regeneration and reuse [35,36].

In addition to heavy metal removal, ENMs can also be engineered as colorimetric sensing platforms for rapid detection in aqueous media. Simple, low-cost, and portable sensing materials capable of providing an immediate visual response are highly attractive for preliminary on-site screening and real-time water quality monitoring [37]. Although established analytical techniques, such as atomic absorption spectroscopy (AAS), inductively coupled plasma optical emission spectroscopy (ICP-OES), inductively coupled plasma mass spectrometry (ICP-MS), and anodic stripping voltammetry (ASV), remain the methods of choice for highly sensitive and quantitative analyses [38], functionalized ENMs can provide a rapid first-level assessment of heavy metal contamination. Contaminated samples can then be subjected to conventional laboratory analyses to verify compliance with regulatory limits.

Herein, thiol-functionalized ENMs are introduced as self-standing, rubber-based materials capable of effective heavy metal detection and removal in aqueous environments. By integrating green suspension electrospinning with photo-induced thiol-ene chemistry, this work establishes a versatile and sustainable platform for the development of advanced membranes capable of both heavy metal adsorption and chemical recognition. The present work focuses on the design, fabrication, and proof-of-concept demonstration of these multifunctional membranes using single-metal systems as a first step toward future evaluation under more complex wastewater conditions

2. Experimental section

2.1. Materials

SBR latex S19 from RESCOM srl was used as the primary electrospinning material; it contains 50 wt% of styrene-butadiene copolymer with an average particle size between 100 and 200 nm, has a $T_g = 6$ °C, and a viscosity at 25 °C of 300 cP. PEO (Mw = 10^6 g/mol) from Sigma-Aldrich was employed as a template polymer to allow the electrospinning process. The tetrafunctional thiol monomer pentaerythritol tetrakis(3-mercaptopropionate) (TETRA), purchased from Bruno Bock, served as a crosslinker and functionalization agent. Ethyl phenyl(2,4,6-trimethyl benzoyl)phenyl phosphinate (TPO-L), provided by IGM Resins Italia, was used as the photoinitiator. The structure of TETRA and TPO-L are drawn in Figure S1 of the Supporting Information. Ellman's reagent 5,5′-dithiobis(2-nitrobenzoic acid) (DTNB) was supplied by Sigma-Aldrich to quantify the amount of available functional groups on the surface of the membranes. Standard heavy metal solutions of Cu(II), Pb (II), Ag(I), and Hg(II) at 1000 mg/L, supplied by Sigma-Aldrich, were used to investigate the detection of heavy metal ions in electrospun nanofibrous membranes. Hydrochloric acid (HCl) from Sigma-Aldrich was used to adjust the pH of the diluted heavy metal solutions. All other chemicals were purchased from Sigma-Aldrich. All materials and chemicals were used without any further purification or modification.

2.2. Electrospun nanofibrous membranes fabrication

The electrospinning suspensions were prepared by combining SBR latex, the polymer template PEO, the photoinitiator TPO-L, and the thiol crosslinker TETRA, using only distilled water as the electrospinning medium. Firstly, PEO powder was dissolved overnight under magnetic stirring in distilled water to obtain 6 wt% aqueous solutions. Subsequently, SBR latex was introduced into the PEO solution at a constant 100/30 (SBR/PEO) weight ratio and mixed for 2 h. In the next step, TPO-L and TETRA were added to the mixture and stirred by a magnetic stirrer for 45 min. The concentration of TPO-L was fixed at 1 phr (parts per hundred rubber), while the crosslinker content varied from 5 to 50 phr relative to the SBR dried content. The composition of the different electrospinning formulations is detailed in Table 1.

The ENMs were fabricated through three consecutive steps: electrospinning, photo-crosslinking, and template removal. First, the electrospinning technique was performed using a horizontal electrospinning setup (E-fiber SKE apparatus) equipped with a syringe tip (inner diameter of 1 mm) and aluminum foil as the substrate. The working voltage was maintained between 16 and 18 kV, the flow rate was set at 0.4 – 0.45 mL/h, and the distance from the spinneret head to the collector was kept at 20 cm. After electrospinning, the membranes were exposed to UV light to crosslink the membrane structure. Irradiation was performed for 10 min at an intensity of 32 mW/cm^2 using the LIGHTNIGHCURE Spotlight Source LC8 (Hamamatsu), which was equipped with an optical fiber. Finally, the membranes were immersed in distilled water for 15 h to remove the PEO template and air-dried under ambient conditions. At the end of the fabrication process, the ENMs were carefully peeled from the substrate, yielding flexible, free-standing fibrous membranes with

Table 1
Composition details of the electrospinning formulations. The unit of measure for each component is phr (parts per hundred rubber), considering the SBR polymer as 100 parts.

Sample	Component concentration (phr)			
	SBR	PEO	TPO-L	TETRA
TETRA05	100	30	1	5
TETRA10	100	30	1	10
TETRA25	100	30	1	25
TETRA50	100	30	1	50

thicknesses of 60–110 μm, depending on the electrospinning duration. The membrane thickness was measured using a digital micrometer, and at least five different points on each membrane were tested to obtain an average value and ensure measurement accuracy.

A continuous thin film (TETRA50_thinfilm) with a thickness of 110 μm, prepared by cast molding using the same TETRA50 composition, was also fabricated to serve as a reference for comparing the properties of the electrospun fibrous membranes with those of the non-fibrous film. After cast molding and water evaporation, the thin film was crosslinked under UV light and subsequently treated with water to remove the template, following the same procedure used for the ENMs.

2.3. Characterization of the electrospun nanofibrous membranes

The morphology of the ENMs was evaluated using a ZEISS Supra 40 Field-Emission Scanning Electron Microscope (FE-SEM). The samples underwent sputter coating with a 15 nm Pt film utilizing a Quorum Q150T ES apparatus before FE-SEM imaging. Quantitative analysis of the average fiber diameter distribution across all membranes was conducted using ImageJ, with approximately 200 random measurements per sample. The surface porosity and average projected pore area of the electrospun membranes were also determined from FESEM images using ImageJ software. FESEM micrographs were converted into binary images by threshold segmentation, and the projected pore regions of the uppermost fiber layer were identified and quantified. Surface porosity was calculated as the ratio of the projected pore area to the total analyzed image area, while the average projected pore area was determined from the identified pore regions.

Attenuated Total Reflectance – Fourier Transform Infrared (ATR-FTIR) spectroscopy was performed using a ThermoFisher Scientific Nicolet iS50 spectrophotometer to investigate the chemical structure of the ENMs before and after the photo-crosslinking process within the 4000 – 500 cm^{-1} spectral range. Additionally, the photo-crosslinking kinetics of all samples were monitored in real time using the same FTIR instrument in transmittance mode, equipped with a liquid nitrogen-cooled mercury-cadmium-telluride (MCT) detector. The conversion percentage of vinyl groups at 910 cm^{-1} was calculated by the decrease of the C═C double bonds peak area as a function of irradiation time (t) (Eq. (1)), where A and A_{ref} represent the peak areas of C═C double bonds and out-of-plane bending of the C—H groups (reference peak) in the aromatic ring, respectively.

$$Conversion\ (\%) = \left(1 - \frac{|A/A_{ref}|_t}{|A/A_{ref}|_{t=0}}\right) x100 \quad (1)$$

Ellman's reagent DTNB method was performed to quantify the amount of active thiol groups available on the membrane surface (Figure S2 of the Supporting Information) [39–41]. The thiol concentration was determined by using the Beer–Lambert law (Eq. (2)):

$$A = \varepsilon bc \quad (2)$$

where A is the absorbance at 412 nm (i.e., the characteristic absorbance peak of DTNB), b is the path length of the cuvette for UV–Vis measurement (1 cm), c is the concentration of the DTNB solution, and ε is the molar absorption coefficient (with a value of 14,1500 $M^{-1}cm^{-1}$) [42]. A DTNB solution with a concentration of 100 μM was prepared by dissolving Ellman's reagent powder in phosphate-buffered saline (0.01 M and pH 7.4). Then, approximately 10 mg (dried weight) of the free-standing membrane was immersed in 20 mL of the testing solution under ambient conditions for 24 h, with gentle agitation to ensure completion of the reaction. UV–Vis spectra were acquired from 200 to 700 nm using an Evolution One Plus UV–Vis spectrophotometer (ThermoScientific). After the UV–Vis measurement, the concentration of available active thiol groups was normalized to the weight of the dried free-standing membrane.

To evaluate the mechanical properties of the ENMs, a Small Tensile Tester Z5 (Thumler GmbH) in uniaxial tensile mode, equipped with a 500 N load cell, was utilized. The membranes were cut into tensile samples with the dimensions of 25 × 10 × 0.12 mm^3. All measurements were performed under ambient conditions at a consistent stretching speed of 5 mm/min. For each formulation, a minimum of four replicate measurements were conducted to ensure statistical validity, from which average values for the tensile stress and strain at break were derived.

The wettability of the ENMs was assessed by measuring the static water contact angle under ambient conditions using an FTA 1000 Drop Shape Instrument (First Ten Angstroms). The reported values were obtained from five independent measurements performed on different areas of the membrane, using bidistilled water (surface tension $\gamma = 72$ mN/m at 25 °C).

2.4. Investigation of heavy metals binding by ENMs

Four heavy metal ions, i.e., Cu(II), Pb(II), Hg(II), and Ag(I), were chosen as model contaminants for evaluating the metal-binding capacity of the ENMs. The heavy metal ion solutions were prepared by diluting a 1000 mg/L standard solution with distilled water to achieve concentrations ranging from 2 to 200 mg/L at pH 1. At low concentrations, the pH value was adjusted by adding dilute HCl to ensure a constant pH 1 across all samples. To evaluate the influence of solution pH on metal uptake, Cu(II) binding experiments were also performed over the pH range 1–6.5 following the same procedure. The free-standing membrane samples (approximately 10 mg, dry weight) were immersed in the prepared heavy-metal ion solutions and maintained under static conditions with gentle agitation for 120 min to promote metal-thiol interactions. After that, the membranes were carefully retrieved, thoroughly rinsed with distilled water, and air-dried in ambient conditions for 24 h. Control experiments were performed by immersing the membranes in distilled water (pH 1) under the same experimental conditions.

The samples were then analyzed using an Evolution One Plus UV–Vis Spectrophotometer (ThermoScientific) equipped with an ISA-220 Integrating Sphere Accessory, operating in total reflectance mode over the wavelength range of 200–700 nm. Moreover, Energy Dispersive X-ray Spectroscopy (EDX, Oxford Inca Energy 450) was used to detect the presence of heavy metals on the membrane surface.

Unless otherwise stated, at least three independent membrane samples were tested for each membrane formulation and experimental condition to assess the reproducibility of the results. For UV–Vis characterization, representative spectra are presented, while the observed spectral features and the corresponding conclusions were confirmed by replicate measurements. Quantitative results are reported as the average of the measurements, and the corresponding standard deviations are provided where applicable.

3. Results and discussion

3.1. Fabrication of the nanofibrous membranes and their characterization

With the aim of producing rubbery ENMs for the detection and removal of heavy metals, shape-stable SBR nanofibrous membranes were fabricated by suspension electrospinning of an aqueous SBR latex containing PEO as a template, a photoinitiating agent, and a tetrafunctional thiol crosslinker (TETRA). Following electrospinning, the membranes were subjected to UV irradiation to initiate photo-induced thiol-ene reactions. The tetrafunctional thiol crosslinker plays a dual role in the fabrication process. First, it enables crosslinking of the SBR matrix through radical-mediated addition of thiol (-SH) groups to the C═C double bonds in the SBR backbone, resulting in the formation of a 3D crosslinked network that imparts structural stability to the rubbery nanofibers. Second, the thiol-ene reaction introduces accessible thiol functional groups on the fiber surface, enabling chemical functionalization without additional post-treatment steps. Subsequently, the PEO

template was selectively removed without compromising the nanofibrous architecture, yielding stable rubber ENMs with surface-exposed active thiol groups. Owing to the strong affinity of thiol functional groups toward heavy metal ions [21,24] the resulting membranes were designed to function both as active sorbents for metal ion removal and as detection platforms in aqueous environments.

The overall process for fabricating the functional rubber ENMs, together with representative optical and FESEM images of the resulting membranes, is schematically illustrated in Fig. 1.

Four different formulations were prepared by varying the crosslinker content from 5 to 50 phr (Table 1). The resulting SBR membranes, named TETRA05, TETRA10, TETRA25, and TETRA50, were fabricated using a standardized electrospinning time of 60 min, yielding membrane thicknesses in the range of 60–70 μm. The comparable thickness values across all formulations indicate consistent deposition rates that are unaffected by formulation composition. Additionally, a linear correlation between electrospinning duration and membrane thickness was observed, suggesting that membrane thickness could be effectively predicted and controlled by adjusting the processing time.

Following electrospinning, the membranes were exposed to UV irradiation, and the progression of the photo-induced thiol-ene reaction was monitored by ATR-FTIR spectroscopy. During irradiation, a progressive decrease in the characteristic absorption bands associated with both reactive species was observed, confirming the occurrence of thiol-ene crosslinking [15,17,20,43]. In particular, the intensity of the C═C double-bond bands at 910 and 962 cm^{-1}, corresponding to vinyl and 2-butene units, respectively, as well as the S-H stretching band at approximately 2565 cm^{-1}, gradually decreased with irradiation time. As a representative example, Fig. 2a shows the ATR-FTIR spectra of the TETRA50 membrane before and after 20 min of UV irradiation. After irradiation, a pronounced reduction in both the thiol and C═C absorption bands is observed, further evidencing the consumption of reactive groups during the crosslinking process (see also Figure S3 in the Supporting Information).

The influence of thiol crosslinker content on the photo-crosslinking kinetics was further investigated by real-time FTIR measurements. Fig. 2b shows the evolution of vinyl group conversion as a function of UV exposure time. Because the thiol absorption band becomes relatively noisy at low crosslinker concentrations, the conversion was quantified using the decrease in the vinyl absorption peak only. All formulations exhibited a rapid increase in conversion within the first minute of irradiation, indicating efficient consumption of vinyl groups under UV exposure. Subsequently, the reaction kinetics reached a plateau region after approximately 10 min of irradiation, indicating the completion of the thiol-ene reaction and the onset of competing processes, such as butadiene homopolymerization, which may occur as thiol groups become depleted or sterically inaccessible [20].

The TETRA05 formulation, containing the lowest amount of crosslinker (5 phr), exhibited the lowest final conversion, reaching only ~40% vinyl group consumption after 20 min of irradiation. In contrast, formulations with a higher amount of crosslinker (10–50 phr) presented a comparable conversion plateau of around 70%, indicating the presence of a critical crosslinker threshold (i.e., the critical thiol concentration required for effective network formation). The similar final vinyl conversions observed for TETRA10, TETRA25, and TETRA50 formulations further suggest that, beyond 10 phr, the thiol-ene reaction proceeds under thiol-excess conditions, thus unreacted -SH groups are expected to be present in the network. This observation provides an initial indication of how formulation composition influences the availability of active thiol groups, which is quantitatively evaluated later in this work in relation to heavy metal binding performance.

Overall, the FTIR analyses confirmed the successful light-mediated thiol-ene reaction, yielding a stable 3D polymer network within the SBR membranes. Since the conversion plateau was reached after approximately 10 min, this irradiation time was selected for membrane fabrication. The formation of a robust network was further supported by the ability to remove the PEO template by simple water washing, as previously reported [15]. The morphology of the resulting ENMs at the end of the fabrication process (i.e., after template removal) was characterized by FE-SEM to confirm membrane integrity and assess the influence of the crosslinker concentration (5–50 phr) on the fiber architecture. Representative FE-SEM images of the surface morphology of ENMs obtained from all four investigated formulations are shown in Fig. 3a–d, while the corresponding fiber diameter distributions are presented in Fig. 3e.

FE-SEM analysis confirmed that all examined samples consisted of

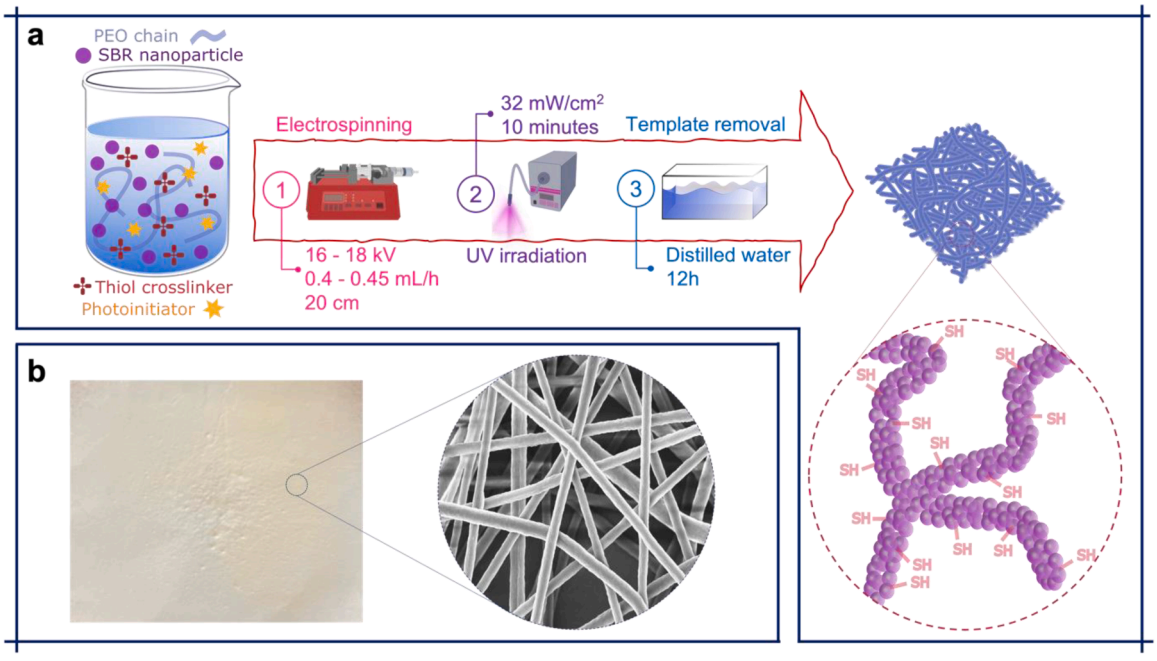


Fig. 1. (a) Schematic illustration of the fabrication procedure of the thiol-functionalized ENMs: (1) suspension electrospinning, (2) UV irradiation, and (3) template removal. (b) Optical photograph of the resulting membrane together with a representative FE-SEM image showing the nanofibrous structure.

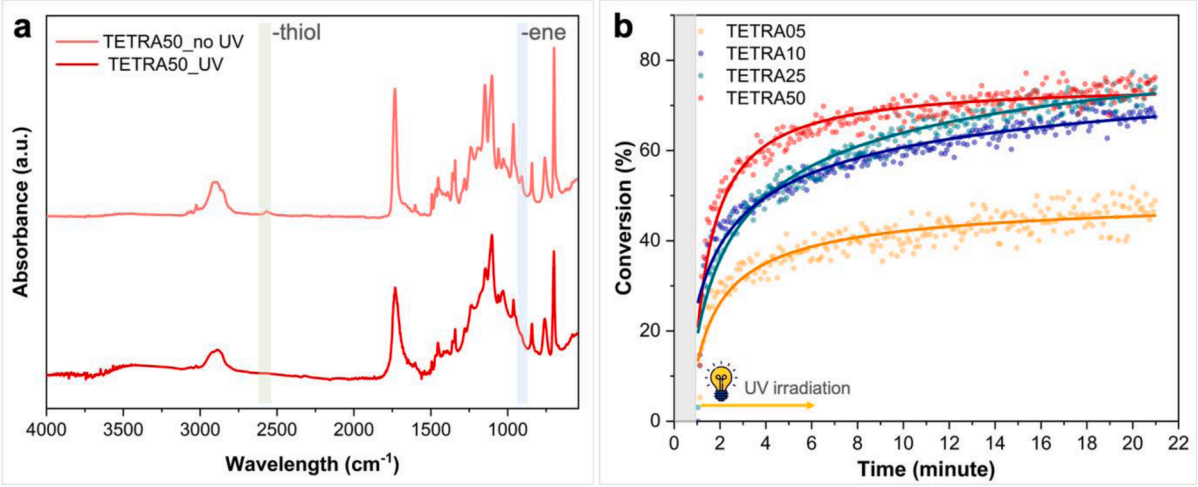


Fig. 2. (a) ATR-FTIR spectra of the membrane containing the highest amount of crosslinker (TETRA50) before (TETRA50_no UV) and after (TETRA50_UV) 20 min of irradiation. (b) Vinyl conversion percentage as a function of irradiation time for all formulations, as determined by real-time FTIR measurements.

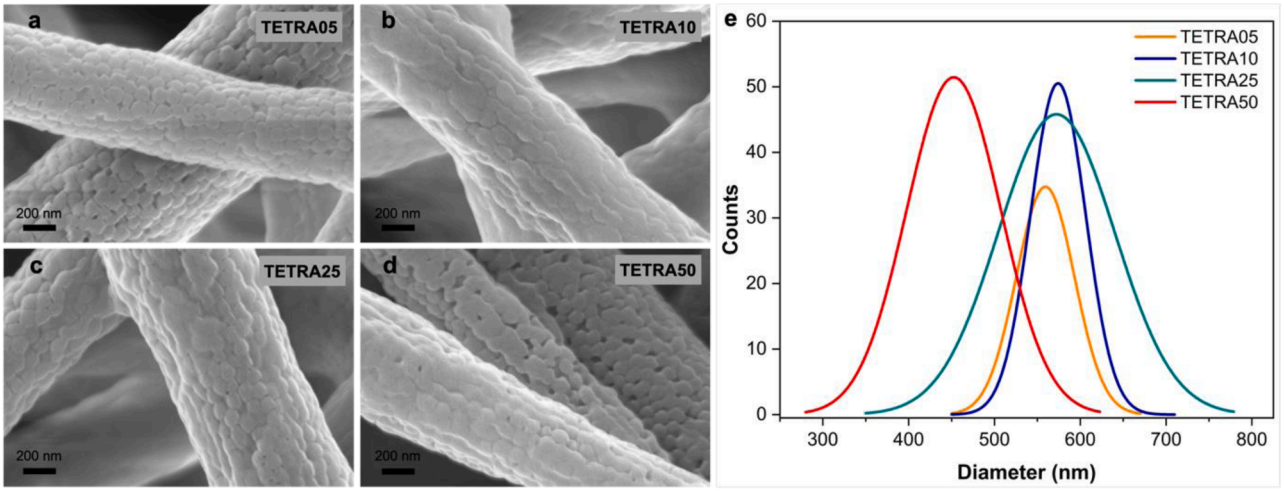


Fig. 3. Morphological analysis of the ENMs with different amounts of thiol crosslinker from 5 to 50 phr: FESEM images of (a) TETRA05, (b) TETRA10, (c) TETRA25, and (d) TETRA50; and (e) corresponding normalized average fiber diameter distributions.

continuous, cylindrical fibers with well-defined borders. No evidence of structural defects, collapse points, or fiber fusion was detected, indicating that the structural integrity of the nanofibrous membranes was preserved via the thiol-ene photo-mediated crosslinking step. Additionally, all fibers exhibited a rough surface morphology, attributed to the assembly of SBR nanoparticles during electrospinning and the subsequent removal of the PEO template.

The TETRA05, TETRA10, and TETRA25 membranes exhibited a comparable average fiber diameter of approximately 550–600 nm. Whereas the TETRA50 formulation produced thinner fibers, with an average diameter of about 450 nm. This reduction in fiber diameter at high crosslinker content could be attributed to the plasticizing or lubricating effect [44] of the thiol crosslinker on the polymer chains. At this concentration, the small TETRA molecules can reduce intermolecular friction, increase chain mobility, and decrease polymer entanglements during electrospinning. As a result, the polymer jet becomes more responsive to elongational forces, leading to enhanced stretching and the formation of thinner fibers.

Considering the intended application of the membranes for heavy-metal ion treatment in aqueous environments, their mechanical integrity and surface wettability were assessed by tensile tests and water contact angle measurements, respectively. Generally, the membranes exhibited comparable mechanical performance despite the wide range of crosslinker concentrations investigated (5–50 phr). The maximum stress ranged from approximately 1.0 to 1.5 MPa, while the strain at break remained below 40% for all formulations (Figure S4 of the Supporting Information). These results indicate that increasing the crosslinker concentration does not significantly affect the mechanical properties of the membranes, suggesting that an effective crosslinked network is already established even at relatively low crosslinker contents.

The wettability of the ENMs was assessed by static and time-dependent water contact angle measurements, as shown in Fig. 4. All samples exhibited an initial hydrophobic behavior, characterized by a water contact angle higher than 90°, due to the intrinsic hydrophobic SBR feature (Fig. 4a). Importantly, variation in crosslinker content did not noticeably affect the initial wettability of the membranes. On the other hand, the time-dependent wetting behavior of the membranes revealed the quick adsorption and lateral spreading of the water droplet on the membrane surface. As illustrated for the TETRA50 sample (Fig. 4b), the water contact angle decreased sharply within a few seconds, from around 107° to 40°. This phenomenon is due to the intrinsic porous micro- and nanostructure of the ENMs, which creates a network of interconnected voids within the fibers. Such a structure facilitates

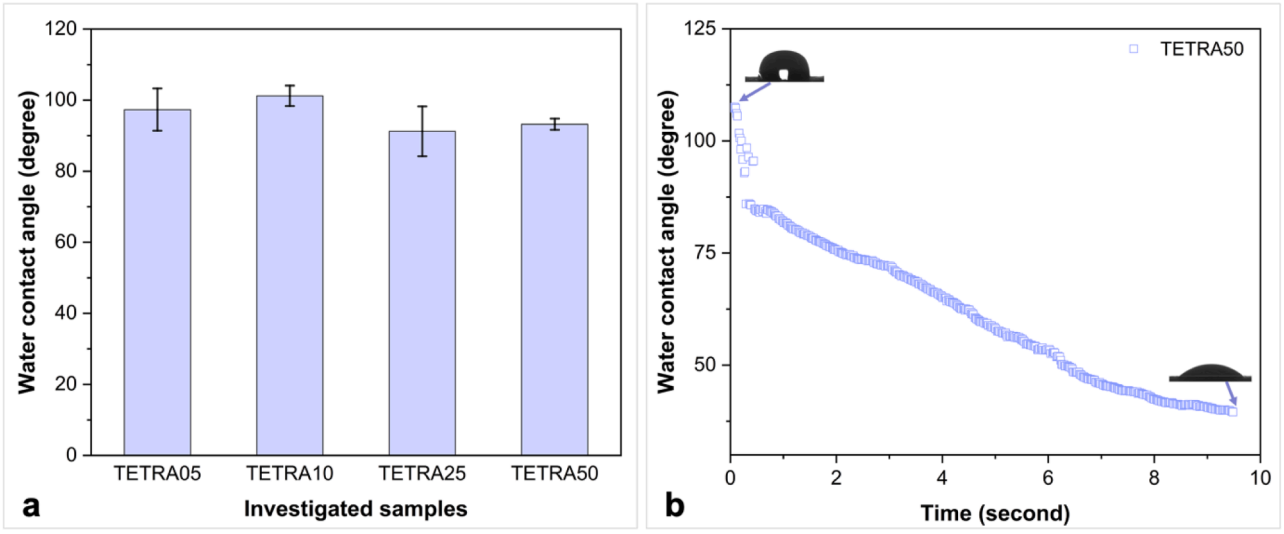


Fig. 4. Wettability of the thiol-functionalized ENMs: (a) water contact angle values of all investigated samples immediately after drop deposition, and (b) the evolution of water contact angle with time of the TETRA50 sample.

capillary-driven water penetration and spreading, effectively increasing the accessible surface area in aqueous environments. This time-dependent hydrophilic property is particularly advantageous for water treatment applications, as it can promote efficient interaction between the membrane surface and dissolved heavy metal ions.

Overall, the combination of stable mechanical properties and favorable wetting behavior across all formulations confirms that these properties are not significantly influenced by membrane composition.

3.2. Quantification of thiol-functionalization and thiol-metal coordination behavior

As the availability of active thiol groups on the membrane are fundamental for heavy metal ions binding, their concentration at the end of the fabrication process was quantified using Ellman's reagent, 5,5′-dithiobis-(2-nitrobenzoic acid) or DTNB. The reaction scheme is reported in Figure S2 of the Supporting Information. In addition to the four investigated ENMs, a continuous thin film with the same composition as TETRA50, produced by cast molding, was also analyzed as a reference to assess the effect of nanofibrous membrane morphology on thiol accessibility. After immersing the membranes and the thin film in the fresh Ellman's reagent solution, all the solutions turned into a yellow coloration of varying intensities (Fig. 5a), qualitatively confirming the presence of surface-accessible thiol groups. The intensity of the yellow coloration increased systematically with increasing thiol crosslinker content, from pale yellow for TETRA05 to intense yellow for TETRA50. Notably, the solution containing the TETRA50 nanofibrous membrane exhibited a significantly higher colour intensity than that of the corresponding thin film, demonstrating enhanced thiol accessibility provided by the nanofibrous architecture compared to a dense, continuous film.

UV–Vis spectra analysis of the DTNB solutions after sample immersion is shown in Fig. 5b. The pristine DTNB solution displayed a single absorption band at approximately 325 nm, corresponding to unreacted DTNB. Following exposure to the samples, a new absorption peak appeared at around 412 nm, attributed to the formation of the yellow-colored 2-nitro-5-thiobenzoate anion (TNB^{2-}), confirming the presence of active thiol groups on the surface of both ENMs and thin-film samples [39,40,45]. For all samples, the coexistence of DTNB and TNB^{2-} absorption bands indicates at the same time the presence of residual unreacted Ellman's reagent and the completion of the thiol-DTNB reaction.

The calculated concentrations of free thiol groups are reported in

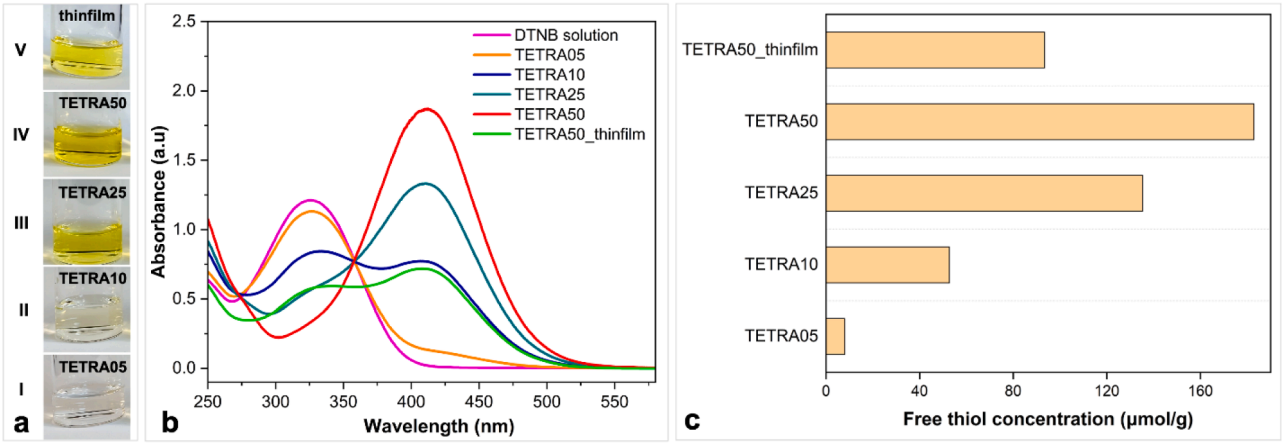


Fig. 5. Quantification of thiol functional group concentrations on the ENMs: (a) photographs of DTNB solution after immersing the functionalized membranes and thin-film (I: TETRA05; II: TETRA10; III: TETRA25: IV: TETRA 50; V: TETRA50_thinfilm); (b) UV–Vis spectra of the DTNB solution prior and after membrane/thin-film immersion, showing the progressive increase of the 412 nm absorption peak, associated with TNB^{2-}, with the amount of the TETRA crosslinker in the electrospinning formulation; (c) free thiol concentration of the functionalized membranes and thin-film normalised by dried sample weight.

Fig. 5c. The TETRA05 sample, which contained the lowest crosslinker content, exhibited only a limited amount of residual thiol groups (around 8 μmol/g), consistent with the low vinyl conversion observed in the rubber matrix (Fig. 2b). This behaviour indicates that, at low crosslinker content, the thiol-ene reaction proceeds nearly to completion, leading to extensive consumption of thiol groups, with only a small fraction remaining unreacted due to steric hindrance or limited accessibility to the unsaturated sites of the SBR backbone. In contrast, membranes fabricated with higher crosslinker contents (TETRA10, TETRA25, and TETRA50) exhibited an excess of thiol functionality, leaving a significant number of unreacted and available thiol groups within the polymer network. Among these samples, TETRA50 membranes provided the highest surface concentration of active thiol groups, reaching approximately 182 μmol/g. These residual thiol groups play a key role in defining the surface reactivity and functional performance of the ENMs toward heavy metal ions.

Although the TETRA50 nanofibrous membrane and the corresponding TETRA50_thinfilm were prepared from the same formulation and exhibited comparable thicknesses, the ENM showed nearly twice the concentration of surface-accessible thiol groups compared to the thin film (≈93 μmol/g). This pronounced difference can be attributed to the advantages of the nanofibrous architecture over a dense, continuous film. FESEM images revealed an interconnected three-dimensional fibrous network composed of overlapping fibers, resulting in an open porous structure. Quantitative image analysis yielded a surface porosity of approximately 34% and an average projected pore area of 44.4 μm^2 (Figure S5 of the Supporting Information), whereas the cast film exhibited a dense morphology with negligible porosity. This open porous architecture increases the accessibility of both external and internal thiol functional groups, thereby promoting more efficient interactions with heavy metal ions.

It is important to consider that the concentration of accessible thiol groups influences not only the adsorption capacity of the membranes but also their sensing performance. A higher density of available thiol groups provides a larger number of coordination sites for heavy metal ions, thereby increasing the probability of metal binding, particularly at low analyte concentrations. Consequently, membranes with higher thiol densities are expected to exhibit improved sensitivity by generating a stronger response for the same metal ion concentration. Nevertheless, the ultimate detection limit is governed not only by the number of available binding sites, but also by both the intrinsic affinity of thiol groups toward the target metal ion and the associated coordination chemistry.

Due to the highest concentration of accessible thiol groups, together with its favorable mechanical integrity and wettability, the TETRA50 membrane was selected for the investigation of thiol–metal coordination and heavy metal detection, as well as for evaluating its potential in water treatment applications. Four representative heavy metal ions, i.e., Cu (II), Pb(II), Hg(II), and Ag(I), were chosen as the target analytes due to their high environmental relevance, widespread occurrence in industrial wastewater, and well-documented yet distinct coordination chemistries and affinities toward thiol functional groups. After the immersion test, the visual appearance of the membranes after exposure is shown in Fig. 6a: the samples exhibited different visual responses depending on the identity of the ion and its coordination chemistry, demonstrating their ion-selective response. After removing the membranes from the heavy-metal ion solutions, the membrane exposed to the copper solution changed its appearance from white to yellow and maintained this color throughout the drying process and storage time. The observed yellow appearance of the membrane could be attributed to the formation of Cu

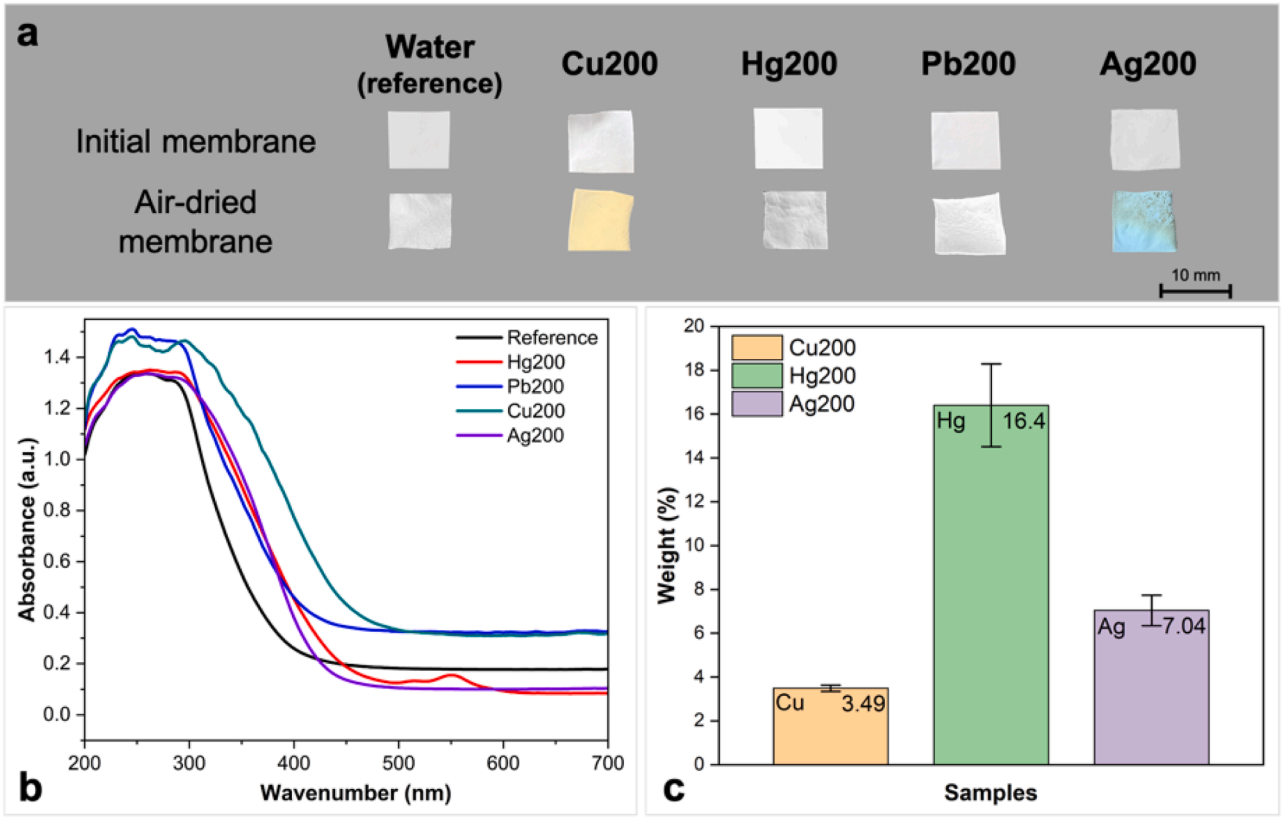


Fig. 6. Thiol-metal coordination of the thiol-functionalized ENMs. (a) Visual appearance of membranes after immersion in aqueous solutions of Cu(II), Hg(II), Pb(II) (concentration of 200 mg/L, pH 1) and subsequent air-drying for 1 day (except for the membrane exposed to Ag(I) solution, which was air-drying for 30 days). (b) Corresponding UV–Vis spectra of membranes after 1 day of air-drying, highlighting ion-dependent spectroscopic responses. (c) Quantitative elemental analysis of heavy metal uptake by the membranes determined by EDX after immersion in the respective metal ion solutions. Error bars represent the standard deviation of three independent experiments.

(II)-thiolate complexes. During coordination, the thiol groups can reduce Cu(II) to Cu(I) while being oxidized to disulfide (-S-S-), leading to the formation of Cu(I)-thiolate complexes, which give the membrane its yellow color (Figure S6 in the Supporting Information) [46–49]. This observation provides direct visual evidence of strong thiol-copper interactions. In contrast, the membranes immersed in mercury and lead solutions retained their original white coloration throughout the experiment and drying process. The unchanged color of these membranes could be attributed to the formation of colorless thiol-metal coordination complexes or to interactions below the visual detection threshold under the tested conditions.

Notably, the membrane exposed to the Ag(I) solution initially remained white after treatment; however, a gradual color transition from white to brown was observed after approximately 20 days of storage under ambient conditions. Fresh Ag(I)–thiolate complexes are typically colorless, explaining the absence of an immediate visual response. Under ambient conditions, however, these complexes can undergo progressive reduction to metallic silver (Ag^0), followed by nucleation and growth of silver nanoparticles, which are responsible for the characteristic brown coloration. This behavior confirms the capture and long-term retention of Ag(I) on the membrane surface. The observed color evolution is likely the result of several concurrent redox pathways promoted by ambient conditions, e.g., exposure to visible and UV light, atmospheric oxygen, moisture. Among these, photo-induced ligand-to-metal charge transfer has been widely reported as one of the principal mechanisms driving the reduction of coordinated Ag(I) species, whereby excitation of the thiolate ligand promotes electron transfer to Ag(I), leading to the formation of metallic silver while the thiol groups are concomitantly oxidized to disulfides (Figure S7, Supporting Information). In addition, direct reduction by residual thiol groups and electron transfer associated with the autoxidation of the unsaturated SBR backbone may also contribute to Ag° formation during prolonged storage [50–52].

The selective binding behavior of the thiol-functionalized ENMs was further investigated by UV–Vis spectroscopy (Fig. 6b), which revealed ion-specific spectroscopic responses consistent with thiol-metal coordination chemistry. Mercury ion detection exhibited the most significant spectroscopic response, with two distinct absorption peaks in the 525–550 nm region. This behavior is attributed to the strong affinity for reduced sulfur functional groups of Hg(II) ions [53]. Typically, Hg(II) forms linear (two-coordinate) complexes with two thiolate ligands, $[Hg(SR)_2]$, and this phenomenon has been attributed to the easy formation of d-s-p hybrid orbitals (ligand-to-metal charge transfer) from the sulfur-based orbitals to the mercury orbital [54]. For the membrane exposed to the copper solution, three characteristic absorption peaks were observed at approximately 230, 250, and 325 nm. The peak at around 230–240 nm represents the free thiol groups still available on the membrane surface, while Cu(II) ions can form copper-thiolate complexes, leading to a peak around 310–330 nm [48]. In this complex formation, the thiol is oxidized to create a thiyl radical, while Cu(II) is reduced to Cu(I). Subsequent recombination of thiyl radicals leads to disulfide bond formation, reflected by an additional absorption feature in the 240–260 nm range, while Cu(I) can be re-oxidized to Cu(II) by oxygen [47]. Similarly, the spectra of the membrane exposed to the Pb(II) solution showed two peaks at approximately 230 and 250 nm, corresponding to free thiol groups and disulfide bonds, respectively, although no visible-region signature peak was detected. In contrast, the membranes exposed to Ag(I) solution exhibited only minimal changes in UV–Vis spectra, consistent with the initially colorless nature of Ag(I)–thiolate complexes.

To directly confirm heavy metal uptake after exposure to the heavy metal ion solutions, the membranes were further analyzed by EDX spectroscopy (Fig. 6c and Figure S8 of the Supporting Information). In this study, EDX was employed as a semi-quantitative surface elemental analysis technique to verify the presence of adsorbed metal ions on the membrane surface rather than to determine adsorption capacity. As shown in Fig. 6c, with the exception of Pb(II), whose signal overlapped with that of sulfur, all investigated metal ions were successfully detected, confirming metal uptake by the thiol-functionalized membranes. Notably, despite the absence of a visible color change, Hg(II)-treated membranes exhibited the highest metal content, reaching approximately 15 wt.%. In comparison, Cu(II)- and Ag(I)-treated membranes showed lower values of approximately 7.5 and 3.5 wt.%, respectively. These results demonstrate that the visual response does not directly correlate with the amount of retained metal, but rather reflects differences in coordination chemistry and electronic structure.

The observed trend is consistent with the Hard and Soft Acids and Bases (HSAB) principle. Thiolate sulfur is a typical soft Lewis base and therefore exhibits preferential interactions with soft Lewis acids, while showing much lower affinity toward hard cations commonly present in natural waters, such as Na^+, K^+, Ca^{2+}, and Mg^{2+} [22]. Among the investigated heavy metal ions, Hg(II) is the softest Lewis acid and consequently forms the strongest Hg–S coordination bonds. Ag(I) also exhibits high affinity toward sulfur-containing ligands, whereas Cu(II) and Pb(II) behave as borderline Lewis acids, resulting in comparatively weaker interactions with thiol groups. This behavior is consistent with the higher Hg content detected by EDX and suggests that common inorganic ions are expected to exert only limited competition for the thiol binding sites.

Since solution pH strongly influences both heavy metal speciation and the protonation state of surface thiol groups, its effect on the interaction between the membrane and Cu(II) was further investigated. The corresponding EDX results are reported in Figure S9 of the Supporting Information and confirm measurable Cu retention on the membrane surface throughout the investigated pH range (1–6.5). The most acidic condition (pH 1) was deliberately selected for the comparative study of Cu(II), Pb(II), Hg(II), and Ag(I) because, under these conditions, all metal ions remain predominantly as free ionic species, minimizing hydrolysis and precipitation phenomena that could interfere with the interpretation of thiol–metal coordination. This enables a direct comparison of the different metal ions under identical solution chemistry. Although the high proton concentration competes with metal ions for thiol binding sites, the strong affinity of soft metal ions toward sulfur-containing ligands still promotes stable thiolate complex formation. As the pH increases, Cu(II) hydrolysis becomes increasingly significant, reducing the concentration of free Cu^{2+} ions available for coordination with surface thiol groups, which is reflected in the lower Cu content detected on the membrane surface. It is also worth noting that highly acidic conditions are representative of several industrial wastewaters, such as acid mine drainage and hydrometallurgical process streams, where efficient heavy metal removal under strongly acidic conditions is of particular importance.

The sensitivity assessment of the ENMs toward Cu(II) was then conducted by varying the copper solution concentration from 200 to 2 mg/L. The concentration-dependent color transition of the membranes and the corresponding UV–Vis spectral evolution are shown in Fig. 7, together with a reference membrane immersed in distilled water. Visual inspection revealed a discernible color change down to a Cu(II) concentration of approximately 10 mg/L (Fig. 7a and b), defining the practical colorimetric detection limit of the thiol-functionalized membrane. At lower concentrations, UV–Vis spectroscopy allowed detection of the copper–thiolate absorption band at 310–330 nm down to approximately 3 mg/L (Fig. 7c), below which the signal became indistinguishable due to insufficient thiol saturation.

Overall, the combined colorimetric response, UV–Vis spectroscopic signatures, and quantitative EDX analysis demonstrate that thiol-functionalized ENMs interact effectively with heavy metal ions through thiol–metal coordination mechanisms. The membranes exhibit dual functionality, acting both as active sorbents and, in the case of Cu (II), as intrinsic colorimetric sensors with concentration-dependent responses. This behavior, together with the high surface accessibility of thiol groups provided by the nanofibrous architecture, highlights their

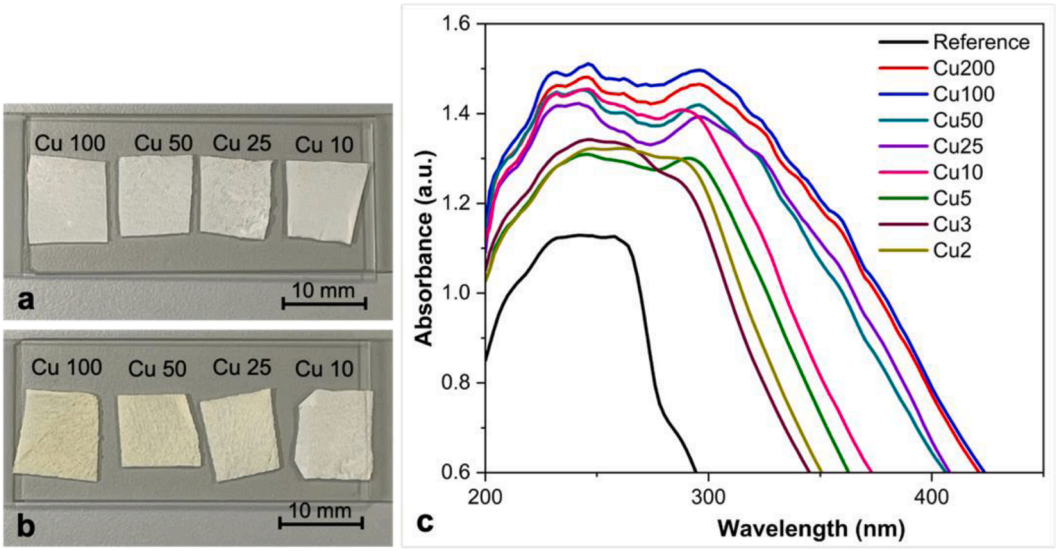


Fig. 7. Concentration-dependent response of thiol-functionalized ENMs toward Cu(II). Appearance of the membranes before (a) and after (b) exposure to the copper solution; (c) corresponding UV–Vis spectra of membranes immersed in Cu(II) solution at different concentrations under ambient conditions, compared to the membrane reference immersed in distilled water.

potential for integrated heavy metal monitoring and remediation in aqueous environments.

From a scalability perspective, the proposed fabrication approach is compatible with industrial processing. Suspension electrospinning from aqueous dispersions can be extended to large-scale production using needleless or roll-to-roll systems, while the use of water as the sole solvent reduces environmental impact and simplifies processing. The combination of commercially available SBR latex and rapid, energy-efficient UV-induced thiol-ene crosslinking further supports integration into continuous manufacturing lines. Overall, the simplicity of the process and tunability of the formulation indicate strong potential for scalable production of functional nanofibrous membranes for water treatment applications.

4. Conclusions

In this work, thiol-functionalized rubber-based electrospun nanofibrous membranes were successfully prepared by integrating suspension electrospinning with photo-induced thiol-ene crosslinking and simultaneous surface functionalization. The resulting membranes exhibit stable nanofibrous structures, tunable surface chemistry, and high densities of accessible thiol groups (up to ~180 μmol/g), enabled by control of the formulation. Compared to dense thin films, the nanofibrous architecture significantly enhances the accessibility of thiol functional groups, highlighting its advantage for surface-driven applications.

The membranes demonstrated ion-dependent interactions with multiple heavy metal ions, combining adsorption capability with intrinsic colorimetric sensing. In particular, Cu(II) detection was achieved with a spectroscopic limit of 3 mg/L.

Overall, the combination of sustainable aqueous processing, tunable thiol surface functionality, robust mechanical and wetting properties, and dual detection–removal capability highlights the potential of these materials for water treatment applications. The simple, solvent-free process and compatibility with scalable electrospinning technologies further support industrial potential.

Future work will focus on quantitative adsorption studies, including adsorption capacity, adsorption kinetics, regeneration, and performance in multicomponent water matrices under environmentally relevant conditions, while further advancing the scalability of the fabrication process toward practical implementation.

CRediT authorship contribution statement

Thi Nhung Vu: Writing – original draft, Visualization, Methodology, Investigation. **Marzia Quaglio:** Writing – review & editing, Methodology. **Roberta Bongiovanni:** Writing – review & editing, Resources, Funding acquisition. **Alessandra Vitale:** Writing – review & editing, Supervision, Project administration, Methodology, Conceptualization.

Declaration of competing interest

The authors declare that they have no known competing financial interests or personal relationships that could have appeared to influence the work reported in this paper.

Acknowledgments

The research work was performed at Politecnico di Torino (POLITO, Italy) within the #horizoneurope2021-2027 programme under the Marie Skłodowska-Curie Doctoral Networks (MSCA-DN) grant agreement No 101073432 (Esperanto project). Funding was provided by the European Union.

Supplementary materials

Supplementary material associated with this article can be found, in the online version, at doi:10.1016/j.ceja.2026.101383.

Data availability

Data will be made available on request.

References

[1] J. Xue, T. Wu, Y. Dai, Y. Xia, Electrospinning and electrospun nanofibers: methods, materials, and applications, Chem. Rev. 119 (8) (2019) 5298–5415, https://doi.org/10.1021/acs.chemrev.8b00593.
[2] A.H. Oleiwi, A.R. Jabur, Q.F. Alsalhy, Electrospinning technology in water treatment applications: review article, Desalination Water Treat. 322 (2025) 101175, https://doi.org/10.1016/j.dwt.2025.101175.
[3] Z. Samavati, A. Samavati, P.S. Goh, A. Fauzi Ismail, M. Sohaimi Abdullah, A comprehensive review of recent advances in nanofiltration membranes for heavy metal removal from wastewater, Chem. Eng. Res. Design 189 (2023) 530–571, https://doi.org/10.1016/j.cherd.2022.11.042.

[4] Y. Cho, J.W. Beak, M. Sagong, S. Ahn, J.S. Nam, I. Kim, Electrospinning and nanofiber technology: fundamentals, innovations, and applications, Adv. Mater. 37 (28) (2025) 2500162, https://doi.org/10.1002/adma.202500162.

[5] B. Bansod, T. Kumar, R. Thakur, S. Rana, I. Singh, A review on various electrochemical techniques for heavy metal ions detection with different sensing platforms, Biosens. Bioelectron. 94 (2017) 443–455, https://doi.org/10.1016/j.bios.2017.03.031.

[6] M.H. Mobarak, A.Y. Siddiky, Md.A. Islam, A. Hossain, M.I.H. Rimon, Md. S. Oliullah, J. Khan, M. Rahman, N. Hossain, M.A. Chowdhury, Progress and prospects of electrospun nanofibrous membranes for water filtration: a comprehensive review, Desalination 574 (2024) 117285, https://doi.org/10.1016/j.desal.2023.117285.

[7] S. Agarwal, J.H. Wendorff, A. Greiner, Use of electrospinning technique for biomedical applications, Polymer 49 (26) (2008) 5603–5621, https://doi.org/10.1016/j.polymer.2008.09.014.

[8] N. Sharples, O. Doustdar, M. Carmona-Cabello, S. Abrishami, J.M. Herreros, A. Sadaghiani, K.D. Dearn, Sustainable textiles through electrospinning: addressing environmental challenges, J. Textile Instit. 117 (2026) 954–973, https://doi.org/10.1080/00405000.2025.2542934.

[9] P. Wagh, Electrospun membranes for batteries. Electrospun and Nanofibrous Membranes, Elsevier, 2023, pp. 521–553, https://doi.org/10.1016/B978-0-12-823032-9.00012-X.

[10] B.H. Arrosyid, A. Zulfi, S. Nur'aini, S. Hartati, A.F. Rafryanto, A. Noviyanto, D. A. Hapidin, D. Feriyanto, K. Khairurrijal, High-efficiency water filtration by Electrospun expanded polystyrene waste nanofibers, ACS Omega 8 (26) (2023) 23664–23672, https://doi.org/10.1021/acsomega.3c01718.

[11] Z. Uddin, F. Ahmad, T. Ullan, Y. Nawab, S. Ahmad, F. Azam, A. Rasheed, M. S. Zafar, Recent trends in water purification using electrospun nanofibrous membranes, Int. J. Environ. Sci. Technol. 19 (9) (2022) 9149–9176, https://doi.org/10.1007/s13762-021-03603-9.

[12] M.A. Martinez, E. González, Strategies to improve the water resistance of nanofibers obtained by suspension electrospinning, Macro Mater. Eng. 310 (12) (2025) e00181, https://doi.org/10.1002/mame.202500181.

[13] Q. Niu, L. Zeng, X. Mu, J. Nie, G. Ma, Preparation and characterization of core-shell nanofibers by electrospinning combined with in situ UV photopolymerization, J. Ind. Eng. Chem. 34 (2016) 337–343, https://doi.org/10.1016/j.jiec.2015.12.006.

[14] S.-S. Kim, H. Ha, C.J. Ellison, Soybean oil-based thermoset films and fibers with high biobased carbon content via thiol–Ene photopolymerization, ACS Sustain. Chem. Eng. 6 (7) (2018) 8364–8373, https://doi.org/10.1021/acssuschemeng.8b00435.

[15] P. Kianfar, A. Bakry, S.D. Vacche, R. Bongiovanni, A. Vitale, Suspension electrospinning of SBR latex combined with photo-induced crosslinking: control of nanofiber composition, morphology, and properties, J. Mater. Sci. 59 (8) (2024) 3711–3724, https://doi.org/10.1007/s10853-024-09416-8.

[16] S. Mitra, A.J. Chakkraborty, A.M. Tareg, T.B. Emran, F. Nainu, A. Khurso, A. M. Idris, M.U. Khandaker, H. Osman, F.A. Alhumaydhi, J. Simla-Gandara, Impact of heavy metals on the environment and human health: novel therapeutic insights to counter the toxicity, J. King Saud Univer. – Sci. 34 (3) (2022) 101865, https://doi.org/10.1016/j.jksus.2022.101865.

[17] C.E. Hoyle, C.N. Bowman, Thiol–Ene click chemistry, Angew Chem. Int. Ed. 49 (9) (2010) 1540–1573, https://doi.org/10.1002/anie.200903924.

[18] D.S. Kazybayeva, G.S. Irmukhametova, V.V. Khutoryanskiy, Thiol-Ene "click reactions" as a promising approach to polymer materials, Polym. Sci. Ser. B. 64 (1) (2022) 1–16, https://doi.org/10.1134/S1560090422010055.

[19] A.B. Lowe, Thiol-ene "click" reactions and recent applications in polymer and materials synthesis, Polym. Chem. 1 (1) (2010) 17–36, https://doi.org/10.1039/B9PY00216B.

[20] A. Vitale, G. Massaglia, A. Chiodoni, R. Bongiovanni, C.F. Pirri, M. Quaglio, Tuning porosity and functionality of electrospun rubber nanofiber mats by photo-crosslinking, ACS Appl. Mater. Interfaces 11 (27) (2019) 24544–24551, https://doi.org/10.1021/acsami.9b04599.

[21] Z. Xia, L. Baird, N. Zimmerman, M. Yeager, Heavy metal ion removal by thiol functionalized aluminum oxide hydroxide nanowhiskers, Appl. Surf. Sci. 416 (2017) 565–573, https://doi.org/10.1016/j.apsusc.2017.04.095.

[22] T.L. Ho, Hard soft acids bases (HSAB) principle and organic chemistry, Chem. Rev. 75 (1) (1975) 1–20, https://doi.org/10.1021/cr60293a001.

[23] F. He, W. Wang, J.W. Moon, J. Howe, E.M. Pierce, L. Liang, Rapid removal of Hg (II) from aqueous solutions using thiol-functionalized Zn-doped biomagnetite particles, ACS Appl. Mater. Interfaces 4 (8) (2012) 4373–4379, https://doi.org/10.1021/am301031g.

[24] P. Biscarini, L. Fusina, G.D. Nivellini, Dissociation and structure of addition compounds between thioethers and mercury(II) chloride, Inorg. Chem. 10 (11) (1971) 2564–2566, https://doi.org/10.1021/ic50105a037.

[25] R.M. Abu Shmeis, Nanotechnology in wastewater treatment. Comprehensive Analytical Chemistry, Elsevier, 2022, pp. 105–134, https://doi.org/10.1016/bs.coac.2021.11.002.

[26] Y. Huang, Y. Miao, T. Liu, Electrospun fibrous membranes for efficient heavy metal removal, J. Appl. Polymer Sci. 131 (9) (2014) 40864, https://doi.org/10.1002/app.40864 app.

[27] A. Pohl, Removal of heavy metal ions from water and wastewaters by sulfur-containing precipitation agents, Water Air Soil Pollut. 231 (10) (2020) 503, https://doi.org/10.1007/s11270-020-04863-w.

[28] N.A.A. Qasem, R.H. Mohammed, D.U. Lawal, Removal of heavy metal ions from wastewater: a comprehensive and critical review, npj Clean Water 4 (1) (2021) 36, https://doi.org/10.1038/s41545-021-00127-0.

[29] A.Q. Jasim, S.K. Ajjam, Removal of heavy metal ions from wastewater using ion exchange resin in a batch process with kinetic isotherm, S. Afr. J. Chem. Eng. 49 (2024) 43–54, https://doi.org/10.1016/j.sajce.2024.04.002.

[30] L.S. Azmi, N. 'Ain Jabit, S. Ismail, K.E.H. Ku Ishak, T.K. Abdullah, Membrane filtration technologies for sustainable industrial wastewater treatment: a review of heavy metal removal, Desalination Water Treat. 323 (2025) 101321, https://doi.org/10.1016/j.dwt.2025.101321.

[31] I. Ali, V.K. Gupta, Advances in water treatment by adsorption technology, Nat. Protoc. 1 (6) (2006) 2661–2667, https://doi.org/10.1038/nprot.2006.370.

[32] M.H. Hashem, M. Hammoud, M.N. Ahmad, M. Hmadeh, Electrospun polyvinyl chloride/UiO-66(COOH)$_2$ nanocomposite membranes for efficient and rapid heavy metal removal, ACS Appl. Mater. Interfaces 17 (10) (2025) 16275–16286, https://doi.org/10.1021/acsami.4c22963.

[33] C.R. Fadila, M.H.D. Othman, M.R. Adam, R. Takagi, T. Yoshida, W. Khongnakom, M.A. Rahman, J. Jaafar, A.F. Ismail, Adsorptive membrane for heavy metal removal: material, fabrication, and performance, Mater. Today: Proc. 65 (2022) 3037–3045, https://doi.org/10.1016/j.matpr.2022.03.582.

[34] M.R. Adam, M.H.D. Othman, T.A. Kurniawan, M.H. Puteh, A.F. Ismail, W. Khongnakom, M.A. Rahman, J. Jaafar, Advances in adsorptive membrane technology for water treatment and resource recovery applications: a critical review, J. Environ. Chem. Eng. 10 (3) (2022) 107633, https://doi.org/10.1016/j.jece.2022.107633.

[35] H. Chen, M. Huang, Y. Liu, L. Meng, M. Ma, Functionalized electrospun nanofiber membranes for water treatment: a review, Sci. Total Environ. 739 (2020) 139944, https://doi.org/10.1016/j.scitotenv.2020.139944.

[36] Y. Tang, Z. Cai, X. Sun, C. Chong, X. Yan, M. Li, J. Xu, Electrospun nanofiber-based membranes for water treatment, Polymers 14 (10) (2004) 2004, https://doi.org/10.3390/polym14102004.

[37] N. Udawaththa, O. Zubak, A. Daninger, R. Page, M. Strini, B. Romero, P. Pathirathna, Advances and opportunities in point-of-care detection of toxic metals: a review of electrochemical and non-electrochemical approaches, Analyst (2026), https://doi.org/10.1039/D6AN00248J.

[38] S.S. Nadumane, R. Biswas, N. Mazumder, Integrated microfluidic platforms for heavy metal sensing: a comprehensive review, Anal. Methods 16 (18) (2024) 2810–2823, https://doi.org/10.1039/D4AY00293H.

[39] M. Moser, R. Schneider, T. Behnke, T. Schneider, J. Falkenhagen, U. Resch-Genger, Ellman's and Aldrithiol assay as versatile and complementary tools for the quantification of thiol groups and ligands on nanomaterials, Anal. Chem. 88 (17) (2016) 8624–8631, https://doi.org/10.1021/acs.analchem.6b01798.

[40] D. Gergel', A.I. Cederbaum, Interaction of nitric oxide with 2-thio-5-nitrobenzoic acid: implications for the determination of free sulfhydryl groups by Ellman's reagent, Arch. Biochem. Biophys. 347 (2) (1997) 282–288, https://doi.org/10.1006/abbi.1997.0352.

[41] A.F.S.A. Habeeb, Reaction of protein sulfhydryl groups with Ellman's reagent, in: Methods in Enzymology, 25, Elsevier, 1972, pp. 457–464, https://doi.org/10.1016/S0076-6879(72)25041-8.

[42] P. Eyer, F. Worek, D. Kiderlen, G. Sinko, A. Stuglin, V. Simeon-Rudolf, E. Reiner, Molar absorption coefficients for the reduced Ellman reagent: reassessment, Anal. Biochem. 312 (2) (2003) 224–227, https://doi.org/10.1016/S0003-2697(02)00506-7.

[43] C. Decker, T. Nguyen Thi Viet, Photocrosslinking of functionalized rubbers IX. Thiol-ene polymerization of styrene-butadiene-block-copolymers, Polymer 41 (11) (2000) 3905–3912, https://doi.org/10.1016/S0032-3861(99)00649-7.

[44] S. Pan, Y. Yan, R. Chen, Z. Zhao, X. Du, X. Shen, R. Shen, Z. Shao, G. Zheng, Small molecule barrier empowered high-efficiency green electrospinning of fully bio-based nanofibrous membrane for antibacterial and UV-shielding air filtration, J. Hazard. Mater. 496 (2025) 139454, https://doi.org/10.1016/j.jhazmat.2025.139454.

[45] R. Schmidt, M.G. Logan, S. Patty, J.L. Ferracane, C.S. Pfeifer, A.J. Kendall, Thiol quantification using colorimetric Thiol–Disulfide exchange in nonaqueous solvents, ACS Omega 8 (10) (2023) 9356–9363, https://doi.org/10.1021/acsomega.2c07792.

[46] L. Pecci, G. Montefoschi, G. Musci, D. Cavallini, Novel findings on the copper catalysed oxidation of cysteine, Amino Acids 13 (3–4) (1997) 355–367, https://doi.org/10.1007/BF01372599.

[47] D. Crmarić, E. Bura-Nakić, Interaction between Cu and thiols of biological and environmental importance: case study using combined spectrophotometric/bathocuproine sulfonate disodium salt hydrate (BCS) assay, Molecules 28 (13) (2023) 5065, https://doi.org/10.3390/molecules28135065.

[48] M.J. Pushie, L. Zhang, I.J. Pickering, G.N. George, The fictile coordination chemistry of cuprous-thiolate sites in copper chaperones, Biochimica et Biophysica Acta (BBA) – Bioenergetics 1817 (6) (2012) 938–947, https://doi.org/10.1016/j.bbabio.2011.10.004.

[49] R.C. Smith, V.D. Reed, and W.E. Hill, Oxidation of thiols by copper(II), phosphorus sulfur, and silicon and the related elements. 90 (1–4) (1994) 147–154, doi: 10.1080/10426509408016396.

[50] X. Zhang, C.W. Yang, H.Q. Yu, G.P. Sheng, Light-induced reduction of silver ions to silver nanoparticles in aquatic environments by microbial extracellular polymeric substances (EPS), Water Res. 106 (2016) 242–248, https://doi.org/10.1016/j.watres.2016.10.004.

[51] M. Harada, E. Katagiri, Mechanism of silver particle formation during photoreduction using in situ time-resolved SAXS analysis, Langmuir 26 (23) (2010) 17896–17905, https://doi.org/10.1021/la102705h.

[52] C.S. Danna, D.G.S.M. Cavalcante, A.S. Gomes, L.E. Kerche-Silva, E. Yoshihara, I. O. Osorio-Román, L.O. Salmazo, M.A. Rodríguez-Pérez, R.F. Aroca, A.E. Job, Silver nanoparticles embedded in natural rubber films: synthesis, characterization, and

evaluation of In vitro toxicity, J. Nanomater. 2016 (2016) 1–10, https://doi.org/10.1155/2016/2368630.

[53] V. Liem-Nguyen, U. Skyllberg, K. Nam, E. Björn, Thermodynamic stability of mercury(II) complexes formed with environmentally relevant low-molecular-mass thiols studied by competing ligand exchange and density functional theory, Environ. Chem. 14 (4) (2017) 243–253, https://doi.org/10.1071/EN17062.

[54] J.G. Wright, M.J. Natan, F.M. MacDonnel, D.M. Ralston, T.V. O'Halloran, Mercury (II)—Thiolate chemistry and the mechanism of the heavy metal biosensor MerR, in: S.J. Lippard (Ed.), Progress in Inorganic Chemistry, 1st ednProgress in Inorganic Chemistry, v38, Wiley, 1990, pp. 323–412, https://doi.org/10.1002/9780470166390.ch6.